Aerosol Radiative Impact on Spectral Solar Flux at the Surface, Derived from Principal-Plane Sky Measurements

Y. J. KAUFMAN,* D. TANRÉ,+ B. N. HOLBEN,* S. MATTOO,# L. A. REMER,* T. F. ECK,@,& J. VAUGHAN,** AND BERNADETTE CHATENET++

*NASA Goddard Space Flight Center, Greenbelt, Maryland
+Laboratoire d'Optique Atmospherique, CNRS, Université de Sciences et Techniques de Lille, Villeneuve d'Ascq, France
#SM&A Corporation, Vienna, Virginia
@Raytheon ITSS, Lanham, Maryland, and NASA Goddard Space Flight Center, Greenbelt, Maryland
**Department of Civil and Environmental Engineering, Washington State University, Pullman, Washington
++Laboratoire Interuniversitaire des Systèmes Atmosphériques, Universités Paris VII et Paris XII, CNRS, Creteil, France

(Manuscript received 15 May 2000, in final form 10 January 2001)

ABSTRACT

Accurate measurements of the spectral solar flux reaching the surface in cloud-free conditions are required to determine the aerosol radiative impact and to test aerosol models that are used to calculate radiative forcing of climate. Spectral flux measurements are hampered in many locations by persistent broken cloud fields. Here a new technique is developed to derive the diffuse solar spectral flux reaching the surface from principal-plane measurements conducted in the last six years by the Aerosol Robotic Network (AERONET). This 50–100 instrument global network measures the principal-plane radiances in four spectral bands (0.44–1.02 μm) approximately every hour every day. These instruments also measure the spectral optical thickness and derive the aerosol size distribution and other properties from sky measurements. The advantage of the AERONET measurements is that collimated sky radiance is measured for each $1° \times 1°$ field of view. Clouds and cloud shadows are rejected before the total sky brightness is reconstructed and the flux is derived. The results compare favorably with shadow band measurements and with aerosol models. Studied are smoke aerosol in Brazil; Saharan dust in Cape Verde; and urban–industrial pollution in Créteil, near Paris, France, and near Washington, D.C. The spectral attenuation of total (diffuse+direct) solar flux reaching the surface is given by $f_\lambda = \exp(-a_\lambda - b_\lambda\tau_\lambda)$, where a_λ is attenuation by an atmosphere with no aerosol and b_λ is the aerosol attenuation coefficient. Remarkably, it is found that for these sites except for the Washington, D.C., site, the spectrally averaged value of b_λ does not vary significantly from one aerosol type to another: $\{b_\lambda\} = 0.35 \pm 0.03$ (for solar zenith angle of 50°). The measured 24-h average aerosol impact on the solar flux at the surface per unit optical thickness is $\Delta F/\Delta\tau = -80$ W m^{-2} in these sites, almost independent of the aerosol type: smoke, dust, or urban–industrial pollution. In Washington, D.C., it is suspected, and demonstrated in a back of the envelope calculation, that the high amount of broken cloudiness and its correlation with the aerosol optical thickness are responsible for the apparent small aerosol forcing at the surface of $\Delta F/\Delta\tau = -50$ W m^{-2}.

1. Introduction

Aerosol particles, for example, desert dust, smoke from biomass burning, and urban–industrial pollution (Kaufman et al. 1997a), can affect the radiation budget and the temperature field by changing the energy balance and distribution of solar radiation in the atmosphere. To understand this radiative forcing of climate, we need to determine the effect of aerosol on absorption and partition of spectral solar radiation between the earth's surface and atmosphere. Aerosol increases atmospheric absorption of solar radiation and reflection of sunlight back to space. Both of these processes reduce the solar radiation reaching the earth's surface. The reflection of radiation to space may counteract the greenhouse warming by cooling the earth system (Charlson et al. 1992). The redistribution of radiation is expected to change the temperature profiles (Alpert et al. 1998), atmospheric stability and possibly cloud formation (Ackerman et al. 2000).

Satellite spectral measurements are used for remote sensing of the presence of aerosol, for example, the effective aerosol optical thickness derived from Advanced Very High Resolution Radiometer (AVHRR) (Husar et al. 1997) and the absorbing aerosol index derived from Total Ozone Mapping Spectrometer (TOMS) (J. R. Herman et al. 1997). New efforts with

& Current affiliation: Goddard Earth Sciences and Technology Center, University of Maryland Baltimore County, Baltimore, Maryland.

Corresponding author address: Dr. Y. J. Kaufman, NASA GSFC, Code 913, Greenbelt, MD 20771.
E-mail: kaufman@climate.gsfc.nasa.gov

© 2002 American Meteorological Society

Unauthenticated | Downloaded 06/16/21 08:18 PM UTC

present satellites [AVHRR; Ocean Color and Temperature Scanner (OCTS); Polarization and Directionality of the Earth's Reflectances (POLDER)] and new satellite missions [Earth Observing System (EOS) moderate resolution imaging spectroradiometer (MODIS); EOS multiangle imaging spectroradiometer (MISR); *Advanced Earth Observing Satellite* (*ADEOS*) Global Imager (GLI)] work toward quantification of remote sensing of aerosol loading (Kaufman et al. 1997a; Tanré et al. 1997; M. Herman et al. 1997; Nakajima et al. 1999; Higurashi and Nakajima 1999). Spectral fluxes are also derived from the measured radiation field by the MODIS instrument on EOS *Terra* (Tanré et al. 1997; Kaufman et al. 1997b). These measurements will provide spectral fluxes at the top of the atmosphere and should be supplemented by measurements of the aerosol attenuation of the spectral solar flux reaching the earth's surface (King 1979; Bird and Riordan 1986; Harrison et al. 1994, Eck et al. 1998).

The difference between the aerosol forcing at the surface and at the top of the atmosphere is the rate of aerosol heating of the lower atmosphere (Satheesh and Ramanathan 2000). Substantial advancement has been made in regard to the broadband partition of solar radiation and measurements of the flux reaching the surface (Charlock and Alberta 1996; Pinker and Laszlo 1992; Christopher et al. 1998). But in order to resolve the present discrepancies between measured and calculated solar fluxes reaching the surface (Li et al. 1995; Arking 1996; Ramanathan et al. 1995; Cess et al. 1995), spectral measurements of the partition of sunlight are required (e.g., Stephens and Tsay 1990; Vogelmann et al. 1998; Pilewskie et al. 1998), see also review by Li et al. (1997). Spectral partition can be used to decide if the additional absorption is due to unresolved water vapor absorption in the near-IR (e.g., Belmiloud et al. 2000), or due to new molecular absorption not detected before, or wrong aerosol absorption model in a specific spectral region.

Here we introduce a new technique to derive the spectral diffuse radiation reaching the surface. This diffuse flux of scattered sunlight in the sky is derived from sky measurements in the principal plane. The method is suitable for the existing measurements by the 50–100 instrument strong global Aerosol Robotic Network (AERONET) of sun/sky radiometers, which began operation in 1992 (Holben et al. 1998; http://aeronet.gsfc.nasa.gov). It is very different from present flux measurements, thus introducing ''a second opinion'' on the effect of aerosol on attenuation of downward spectral radiation, and an inexpensive method to expand the coverage of the spectral flux measurements. We first describe the pros and cons of the new method and its application to several AERONET prime sites.

2. The remote sensing approach

Remote sensing of the effect of aerosol on the diffuse solar flux reaching the surface is illustrated here using the single scattering approximation for an atmosphere with only aerosol particles, with a scattering phase function $P(\Theta)$ and single scattering albedo ω_0. Application of the method to AERONET data is done using rigorous radiative transfer calculations (Dave and Gazdag 1970) for realistic atmosphere. In the single scattering approximation, for a nonreflective surface, the radiance reaching the surface is given by linearizing the single scattering expression of Hansen and Travis (1974):

$$L_{\text{sky}}(\theta, \theta_0, \phi) = F_0 \omega_0 P(\Theta) \tau / 4 \cos(\theta), \quad (1)$$

where, F_0 is the extraterrestrial solar spectral irradiance, τ the optical thickness and θ is the view zenith angle. The scattering angle Θ is related to the view zenith angle θ, the solar zenith angle θ_0, and the azimuth between them ϕ by

$$\cos(\Theta) = \cos(\theta_0) \cos(\theta) + \sin(\theta_0) \sin(\theta) \cos(\phi). \quad (2)$$

Aerosol properties that determine sky brightness are the single scattering albedo, the phase function and the optical thickness. Though the optical thickness can be accurately derived from the measured attenuation of direct sun light (e.g., Shaw 1979), the phase function and single scattering albedo are much more uncertain (Dubovik et al. 2000).

The diffuse flux reaching the surface is the integral of the sky radiance [Eq. (1)] on the downward hemisphere:

$$F_{\text{sky}} = \int\int L_{\text{sky}}(\theta, \theta_0, \phi) \sin(\theta) \, d\theta \, d\phi. \quad (3)$$

It is measured directly by the shadow band flux instruments, which measure the sky brightness by shadowing the sun (Bush and Valero 1999). Though measurement of the flux is a direct determination of the diffuse solar radiation reaching the surface, it is sensitive to the ability of the instrument to sense equally photons arriving from all directions and requires a perfect horizon line. To derive the aerosol effect on the diffuse flux, it requires perfectly cloud-free conditions. Therefore, the sampling may be biased toward measurements during high pressure systems that suppress cloud activity, but may have atypical aerosol and humidity conditions.

The AERONET autonomous robots record the sky brightness in the principal plane, a plan perpendicular to the surface that passes through the sun. The sky radiance in this plane, similar to Eq. (1), can be described by

$$L_{\text{pp}}(\theta, \theta_0, \phi) = F_0 \omega_0 P_{\text{pp}}(\Theta) \tau / 4 \cos(\theta). \quad (4)$$

Though the principal plane does not cover all the azimuthal angles of the sky it does cover all the scattering angles that determine all of the values of the phase function that affect the sky brightness. Figure 1 demonstrates the distribution of the scattering angle. Note that any scattering angle in the 2D sky can be found by interpolating two values in the 1D principal plane. This full coverage of all the possible scattering angles is the

Unauthenticated | Downloaded 06/16/21 08:18 PM UTC

θ / ϕ	0	20	40	60	80	100	120	140	160	180
0	**60**	60	60	60	60	60	60	60	60	**60**
10	**50**	51	53	55	59	62	65	68	69	**70**
20	**40**	42	46	52	59	65	71	76	79	**80**
30	**30**	33	40	49	59	69	77	84	88	**90**
40	**20**	25	36	49	61	73	84	92	98	**100**
50	**10**	19	34	49	64	78	91	101	108	**110**
60	**0**	17	34	51	68	83	97	109	117	**120**
70	***10***	21	37	55	72	88	104	117	126	**130**
80	***20***	27	42	59	76	93	110	124	136	**140**
90	***30***	36	48	64	81	99	116	132	144	**150**

FIG. 1. Distribution of the scattering angle across the sky as a function of the view zenith angle (θ) and the azimuth (ϕ). Any scattering angle in the sky (e.g., the value of 52° in the box) can be found by interpolation on two adjacent values in the principal plane (e.g., the double-sided box).

basis for using the principal-plane radiances to derive the full sky illumination. It assures that all the physical and chemical parameters that determine the optical properties of the aerosol and the sky radiance are included in the principal-plane radiance. The following steps describe the method.

- Derive the aerosol optical thickness, $\tau_{a'}$ from the AERONET measured attenuation of direct sunlight.
- Calculate an arbitrary sky illumination $L_a(\tau, \rho, \theta, \phi)$ assuming a given aerosol model, for example, a lognormal distribution of spherical homogenous aerosol particles with mean particle radius of $R_g = 0.06$ μm, standard deviation of $\sigma = 0.6$, single scattering albedo of $\omega = 0.98$, refractive index of $1.53-0.003i$, and constant surface reflectance of $\rho = 0.1$. In the single scattering approximation $L_a(\tau, \rho, \theta, \phi)$ is $L_a(\theta, \theta_\phi, \phi) = F_0 \omega_{0a} P_a(\Theta) \tau_a / 4 \cos(\theta)$, where $\omega_{\phi a}$ and $P_a(\Theta)$ are the results of the arbitrary aerosol model and τ_a is the optical thickness derived from the solar measurements.
- Convert the arbitrary sky radiance, $L_a(\tau, \rho, \theta, \phi)$, into the true sky radiance, $L_s(\tau, \rho, \theta, \phi)$, by scaling it with the radiance measured in the principal plane, $L_{pp\text{-}m}(\Theta)$:

$$L_s(\tau, \rho, \theta, \phi) = L_a(\tau, \rho, \theta, \phi)[L_{pp\text{-}m}(\Theta)/L_{pp\text{-}a}(\tau, \Theta)], \quad (5)$$

where $L_{pp\text{-}a}(\Theta)$ is the value of L_a in the principal plane, and Θ is scattering angle for θ, ϕ [see Eq. (1)]. In the single scattering approximation Eq. (5) means

$$\begin{aligned} L_s(\tau, \theta, \phi) &= L_a(\tau, \theta, \phi)[L_{pp\text{-}m}(\Theta)/L_{pp\text{-}a}(\tau, \Theta)] \\ &= (F_0/4) \cdot [\omega_{0a} P_a(\theta, \phi) \tau_a / \cos(\theta_{sky})] \\ &\quad \times [\omega_{0m} P_m(\Theta) \tau_m / \cos(\theta_{pp})] \\ &\quad \div [\omega_{0a} P_a(\Theta) \tau_a / \cos(\theta_{pp})], \quad \text{or} \end{aligned}$$

$$L_s(\tau, \theta, \phi) = F_0 \omega_{0m} P_m(\theta, \phi) \tau_m / 4 \cos(\theta_{sky}), \quad (6)$$

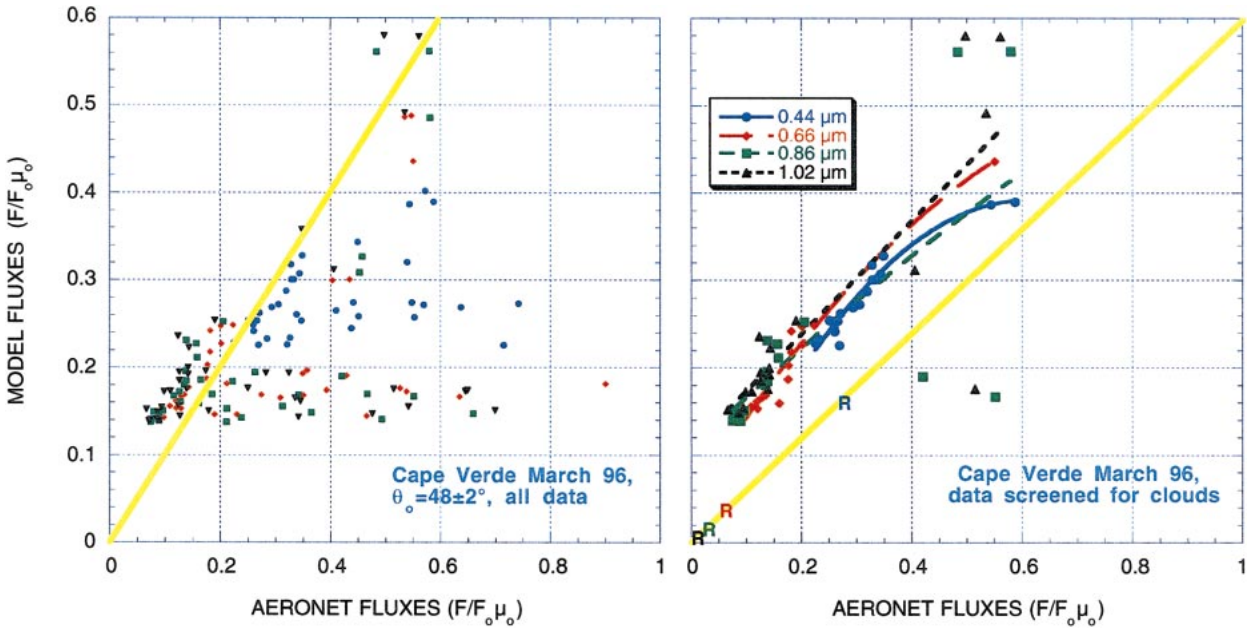

FIG. 2. Effect of cloud screening on the results from Cape Verde. (left) Scatterplot of model fluxes for a simplified one lognormal size distribution with particle effective radius 1.5 μm, refractive index $n_r = 1.53$–0.003 for 0.44 μm and 1.53–0.0 for wavelength larger than 0.6 μm, vs fluxes derived from the AERONET algorithm for all the data. (right) The same results, but after deselecting data with roughness parameter $\sigma_{\lambda i} > 10\%$ at 0.44 and 0.67 μm and $\sigma_{\lambda i} > 20\%$ at 0.86 and 1.02 μm. The Rayleigh value is shown by the letter "R" in the proper color. The measured fluxes are normalized by F/F_ϕ, where F_ϕ is the solar flux in the spectral channel. Only couple of points, evidently contaminated by clouds, were not used in the slope calculations.

Unauthenticated | Downloaded 06/16/21 08:18 PM UTC

TABLE 1. Summary of the accuracy in derivation of the diffuse solar flux reaching the surface from the AERONET radiances measured in the principal plane. The errors are calculated by assuming that the atmospheric aerosol has a lognormal distribution of spherical homogenous aerosol particles with mean particle radius $R_g = 0.06$, std dev $\sigma = 0.6$, single scattering albedo $\omega_0 = 0.98$, refractive index 1.53–0.003*i*, optical thickness of 1.0, and surface reflectance $\rho = 0.1$. The atmosphere is simulated by changing the assumed model to $R_g = 1.0$, $\omega_0 = 0.85$, $\rho = 0.2$ one step at a time, and all steps combined. Viewing angle $\theta_0 = 30°$ and $\lambda = 0.64$ μm.

Change in parameter	Error (%)
Error in particle size, $R_g = 0.06 \rightarrow 1.0$	1.5
Error in surface reflectance, $\rho_s = 0.1 \rightarrow 0.2$	0.7
Error in single scattering albedo, $\omega = 0.98 \rightarrow 0.85$	0.7
Error in aerosol optical thickness, $\Delta\tau = 0.05$	0.7
Error due to aerosol height $H = 1 \rightarrow 3$ km for $\omega = 0.85$	0.3
Standard error	2.4
Combined error:	
$\Delta\tau = -0.05$, $\Delta\rho = 0.1$, $\Delta R_g = 0.94$, $\Delta\omega = -0.13$	0.9

which is the ''true'' 2D distribution of sky brightness. Here ω_{0m} and $P_m(\theta, \phi)$ are the exact, though unknown, quantities in the sky. Therefore, in the single scattering approximation the scaling removed any memory of the assumed aerosol properties. Multiple scattering can be expected to retain some of the memory for these properties.

- Integrate the measured radiance $L_s(\tau, \rho, \theta, \phi)$ to get the derived or measured diffuse sunlight flux reaching the surface:

$$F_{\text{sky}} = \int\int L_s(\tau, \rho, \theta, \theta_0, \phi) \sin(\theta)\, d\theta\, d\phi. \quad (7)$$

The effect of multiple scattering on errors in the scaling [Eq. (5)] is proportional to the aerosol optical thickness. Therefore a sensitivity study is performed for optical thickness of 1.0, using rigorous radiative transfer model, to calculate the residual error. Smaller optical thicknesses are expected to generate proportionally smaller errors. Table 1 summarizes the results. Assuming that the errors are independent, the total error is expected to be smaller than 2.5%. This is substantially smaller than calibration errors of radiometers, or errors introduced in direct spectral flux measurements. Therefore the new method, of deriving the diffuse solar flux on the earth's surface from the measured principal-plane sky radiation is very attractive. As in any method that derives properties of the atmosphere in cloud-free conditions, cloud screening is a critical element. It is described in the next section.

3. Cloud screening

Cloud screening is mainly based on the angular smoothness of the principal plane data. Using data collected from Cape Verde, off the west coast of Africa, during one month, we use the following cloud screening. Define the roughness parameter, $\sigma_{\lambda i'}$ for wavelength λ and scattering angle Θ_i as

$$\sigma_{\lambda i} = 100\% \cdot [L_\lambda(\Theta_{i+1}) + L_\lambda(\Theta_{i-1}) - 2L_\lambda(\Theta_i)]/2L_\lambda(\Theta_i), \quad (8)$$

where $L_\lambda(\Theta_i)$ is the sky radiance in the principal plane for spectral channel λ and scattering angle Θ_i. Data points are eliminated as cloudy if the average of the absolute smoothness parameter $\sigma_{\lambda i}$ is larger than 10% at 0.44 and 0.67 μm and 20% at 0.86 and 1.02 μm. Cloudy data are deselected for each spectral channel separately. The difference accounts for the much darker sky in the near-IR from that in the visible. The thresholds were determined empirically for dust (Fig. 2) and found appropriate for the other aerosol types. Figure 2 demonstrates this cloud screening. Here the fluxes determined from the AERONET measurements are compared with a reference dust model with a simplified one lognormal size distribution with particle effective radius 1.5 μm. The effect of clouds in enhancing the fluxes determined from the AERONET data is evident on the left side of the figure. The cloud screening procedure eliminated most of the cloudy cases.

4. Application

Are the fluxes derived from the AERONET principal plane measurements in agreement with direct flux measurements and with the aerosol physical models? The next several figures address this issue for several aerosol types: smoke, dust, and urban–industrial pollution. Figure 3 shows a comparison between two measurements and one estimate of the spectral diffuse solar flux reaching the surface in Cuiabá, Brazil, during the Smoke, Clouds And Radiation-Brazil (SCAR-B) experiment, in 1995:

- shadow band measurements (open symbols),
- smoke aerosol model [Remer et al. (1998)—full symbols], and
- fluxes derived from the AERONET data (abscissa).

For the range of aerosol optical thicknesses of 0.1 to 0.6 (dashed vertical lines in the figure) for which the smoke aerosol model was developed, there is an excellent agreement with the AERONET data. The shadow band fluxes are systematically lower by $\Delta F/F_0 = 0.06$ from the AERONET measurements. While the correlation between the flux derived from AERONET data and the flux measured by the shadow band is high ($r = 0.90$), the correlation of the AERONET data with the model is much higher ($r = 0.98$). This is mainly due to the much better ability for cloud screening in the AERONET data than in the shadow band. While shadow band measures the whole sky in one shot, AERONET measures each $1° \times 1°$ of sky brightness at a time in the principal plane, and the software eliminates points

Unauthenticated | Downloaded 06/16/21 08:18 PM UTC

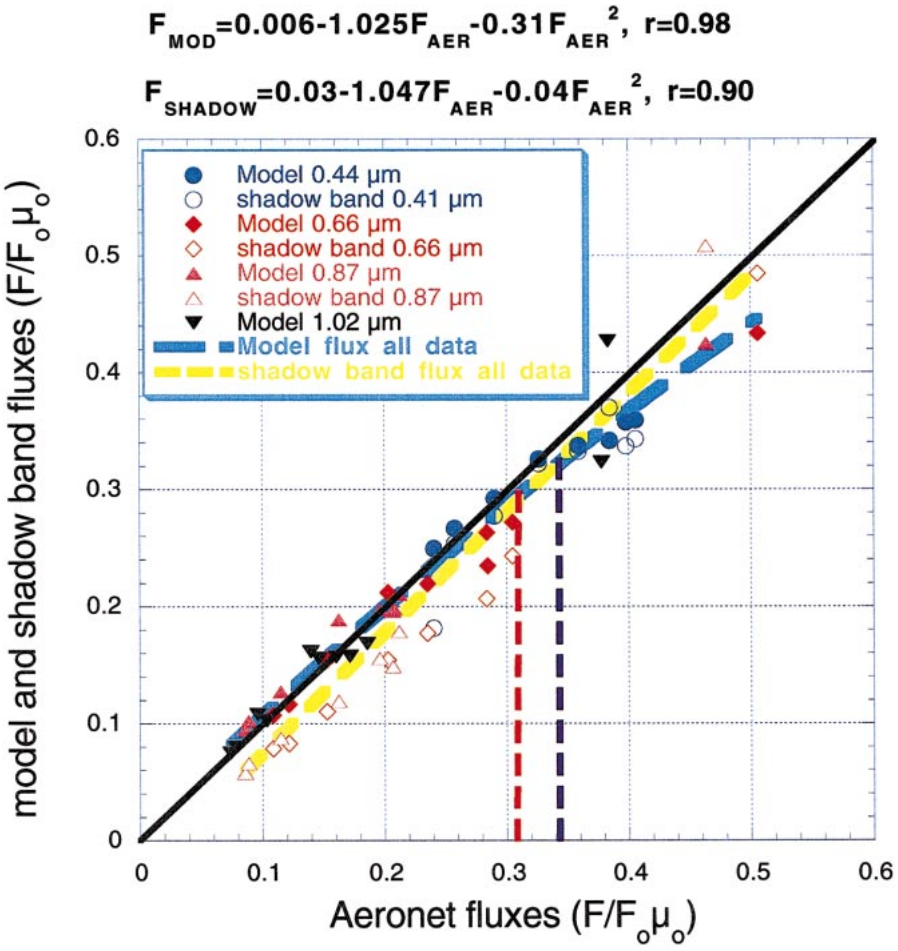

FIG. 3. Comparison between AERONET fluxes from Cuiabá, 1995, and two estimates of the spectral flux at the surface: 1) shadow band measurements (empty symbols), 2) prediction of the fluxes by the smoke aerosol model (full symbol) of Remer et al. (1998). Solar zenith angle is 50°. For the range of aerosol optical thicknesses of $\tau = 0.1$ to 0.6 for which the smoke aerosol model was developed, there is an excellent agreement with the AERONET data. The AERONET flux that corresponds to $\tau = 0.6$ is shown by the dashed lines, for the red and blue channels, respectively. Note that the shadow band first wavelength is shorter than the AERONET. The shadow band fluxes are systematically lower by $\Delta F(\pi/F_0) = 0.06$ from the AERONET measurements.

that are much brighter (cloud) or darker (shadow) than the adjacent points.

We consider it a partial experimental confirmation (for optical thickness <0.6) of the method to derive the fluxes from the AERONET principal plane measurements, since the smoke aerosol model was heavily verified against in situ and radiation measurements (Remer et al. 1998). Remer et al. model is based also on AERONET measurements in Brazil, but in a different time period and on analysis of the almucantar measurements.

A very interesting behavior of the downward diffuse solar flux is shown in Fig. 4. As the aerosol optical thickness increases, it can be expected that the diffuse solar flux to the ground will first increase, reaching a maximum and then decrease. For optical thicknesses less than 1.0, atmospheric scattering transfers photons from the direct solar beam to the diffuse flux, giving the sky its brightness and color. For higher optical thickness, aerosol absorption and backscatering to space decreases the already large diffuse flux, eventually reaching darkness experienced under a heavy dust storm or smoke from a wild fire. The optical thickness for which the sky brightness reaches the maximum value is determined by the aerosol single scattering albedo and backscatering coefficient (Kaufman and Holben 1996). The data indicate higher diffuse sunlight than the model, mainly for high optical thickness. This may be due to higher single scattering albedo, or smaller backscattering coefficient. Sky heterogeneity, discussed later, may also contribute to this difference.

The main purpose of measuring the downward fluxes is to estimate the aerosol radiative impact at the surface. When combined with satellite estimate of radiative impact at the top of the atmosphere, a full impact on the

Unauthenticated | Downloaded 06/16/21 08:18 PM UTC

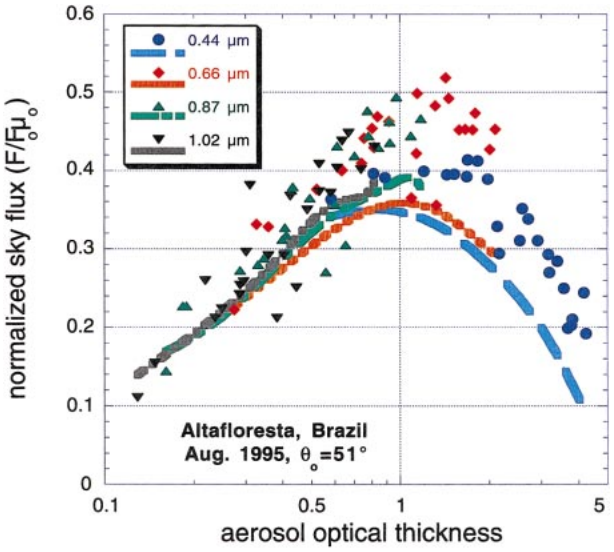

FIG. 4. Solar diffuse fluxes reaching the earth's surface at Alta Floresta, Brazil, as a function of the smoke optical thickness. Data are for the 1995 SCAR-B experiment. The symbols stand for the AERONET data and the lines for the smoke model of Remer et al. (1998).

radiative budget can be achieved. Aerosol backscattering to space reduces the fraction of sunlight absorbed in the atmosphere and by the surface. Therefore increase in anthropogenic aerosol can extract a significant negative forcing at the top and bottom of the atmosphere. Aerosol decreases the absorption of sunlight by the surface but increases the absorption by the atmosphere, thus an increase in the aerosol absorption is a negative forcing at the surface but positive at the top of the atmosphere. The aerosol spectral radiative impact at the surface is proportional to the fraction of spectral sunlight reaching the surface that is derived as the sum of the direct and diffuse fluxes normalized by the solar spectral flux at the top of the atmosphere ($F_0\mu_0$). This fraction, f, is given by

$$f = F_{\text{sky}}/F_0\mu_0 + \exp(-\tau/\mu_0), \tag{9}$$

where the first element on the right is the diffuse component of sunlight reaching the surface and the second term is the direct component. The results for four spectral channels and four locations are given in Fig. 5. Dust in Cape Verde attenuates the solar radiation slightly less than smoke in Brazil (Cuiabá and Alta Floresta), for the same optical thickness. Urban–industrial pollution aerosol was measured on the roof in Goddard Space Flight

TABLE 2. Attenuation of sunlight reaching the earth's surface for solar zenith angle of 50°. The fraction of solar radiation reaching the surface is fitted with an exponential function: $f_\lambda = \exp(-a_\lambda - b_\lambda\tau)$, where a_λ is attenuation by aerosol free atmosphere: $a_{0.44} = 0.17$; $a_{0.67} = 0.033$; $a_{0.87} = 0.009$; $a_{1.02} = 0.003$) and b_λ is the aerosol attenuation given in the table. Results are given for the attenuation functions derived from the AERONET principal-plane radiances, and compared with dust (Tanré et al. 2000), smoke (Remer et al. 1998) and urban–industrial models (Remer and Kaufman 1998). The spectrally averaged $\{b_\lambda\}$ and the Ångström exponent, α, average and standard deviations are also shown.

Models measurements					
Smoke model		Cuiaba		Alta Floresta	
Wavelength	b_λ	Correlation	b_λ	Correlation	b_λ
0.44	0.54	0.92	0.35	0.97	0.37
0.66	0.57	0.89	0.35	0.95	0.39
0.86	0.51	0.86	0.38	0.92	0.43
1.02	0.46	0.79	0.34	0.85	0.35
Average $\{b_\lambda\}$	0.52		0.36		0.38
α (avg, std)	1.8		1.6 ± 0.4		1.2 ± 0.1
Dust model		Cape Verde			
Wavelength	b_λ	Correlation	b_λ		
0.44	0.51	0.38	0.28		
0.67	0.4	—	0.39		
0.86	0.29	0.66	0.34		
1.02	0.27	0.54	0.28		
Average $\{b_\lambda\}$	0.37		0.32		
α (avg, std)	0.5		0.4 ± 0.3		
Urban aerosol		Créteil		GSFC	
Wavelength	b_λ	Correlation	b_λ	Correlation	b_λ
0.44	0.28	0.71	0.32	0.48	0.062
0.67	0.54	0.8	0.42	0.78	0.3
0.86	0.5	0.79	0.26	0.48	0.16
1.02	0.51	0.73	0.33	0.48	0.24
Average $\{b_\lambda\}$	0.46		0.33		0.19
α (avg, std)	1.8		1.4 ± 0.2		1.7 ± 0.2

Unauthenticated | Downloaded 06/16/21 08:18 PM UTC

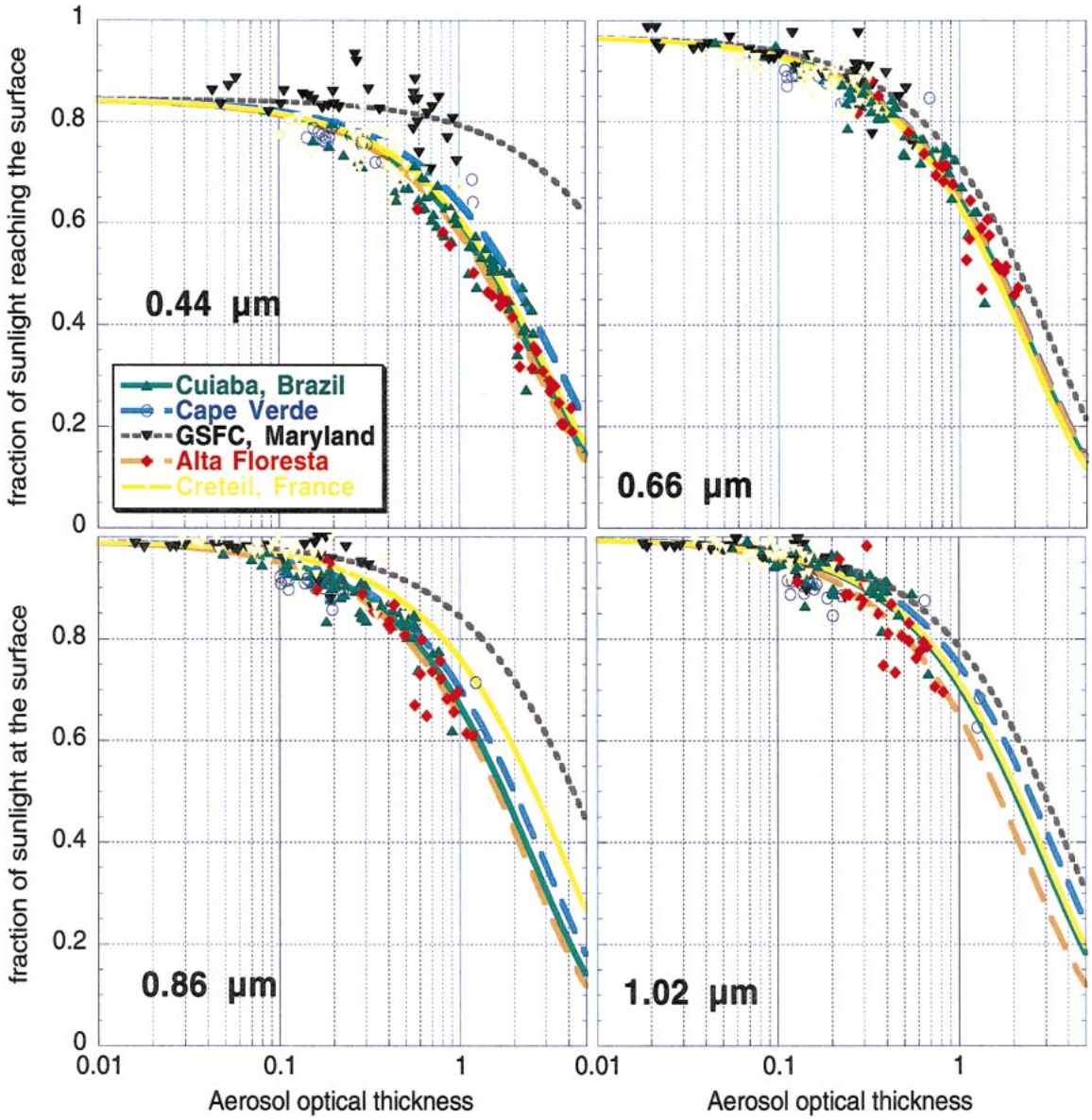

FIG. 5. Attenuation of solar radiation reaching the earth's surface. Results are given for the four AERONET spectral bands, for three locations as a function of the aerosol optical thickness. The solar zenith angle is around 50°. Note that dust in Cape Verde attenuates the solar radiation less than smoke in Brazil (Cuiabá and Alta Floresta). The numerical fits of the data to a transmission function, $f = \exp(-a - b\tau)$, are given in Table 2. Only b is allowed to value, a is fixed based on the Rayleigh scattering value.

Center (GSFC) in Maryland, near Washington, D.C., and in Créteil, France, near Paris. Since the single scattering albedo is higher for urban–industrial pollution (Hegg et al. 1997) than for smoke (Kaufman et al. 1998), it is expected to see a higher fraction of sunlight reaching the surface for a given optical thickness (see model results in Table 2). While the results for Créteil behave according to this rational, aerosol attenuation of the total solar flux in GSFC is very small, with largest discrepancy at 0.44- and 0.86-μm channels. From the scatter of the data it is evident that at least some of this trend is due to sky heterogeneity, For example, the presence of clouds outside the principal plane that enhance its illumination or variation in the relative humidity. Sky heterogeneity can affect the fraction of sunlight reaching the surface for the same aerosol average loading, similar to the effects with broken clouds (Marshak et al. 1997). The experimental data are approximated by an exponential function:

$$f_\lambda = \exp(-a_\lambda - b_\lambda \tau), \tag{10}$$

where a_λ is the Rayleigh attenuation, and b_λ is the aerosol attenuation. Best-fit values of b_λ are given in Table 2. The measured attenuation of spectral sunlight by the

Unauthenticated | Downloaded 06/16/21 08:18 PM UTC

aerosol is smaller by 15%–30% from the theoretical models. However, in GSFC the attenuation is less than half of the model value.

The data in GSFC deviate significantly from the urban–industrial model of Remer and Kaufman (1998) and therefore require further analysis. To decide if the discrepancy between the model and the AERONET data can be due to residual, unresolved clouds, the spectral dependence of the sky fluxes, given by the sky Ångström exponent, α_L: $\alpha_L = \ln(F_1/F_2)/\ln(\lambda_1/\lambda_2)$ is shown in Fig. 6. For AERONET and the model we use $\lambda_1 = 0.44$, $\lambda_2 = 1.02$ μm. A very good agreement is found between the values of the sky Ångström exponent for AERONET and the model. The Ångström exponent should be zero, or even negative for clouds. So it is not possible that the differences observed in Fig. 5 are due to unresolved clouds in the field of view. We ruled out the effect of uncertainty in the real refractive index that is strongly affected by the inclusion of liquid water in high humidities. Note that the attenuation of solar radiation reaching the surface in Créteil show much better agreement with the urban–industrial model (Fig. 7) than the GSFC data. The main difference in the data from Créteil and GSFC is the presence of broken cloudiness in GSFC that caused a rejection of 55% of the data versus 10% in Créteil. The GSFC data are further analyzed in the discussion section.

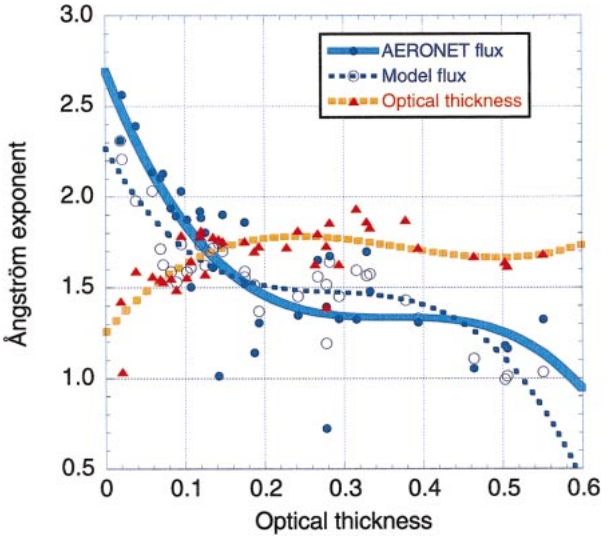

FIG. 6. The Ångström exponent, α_F, describing the spectral properties of the sky flux as measured by AERONET and predicted by the urban–industrial model. It is defined as $\alpha = \ln(F_1/F_2)/\ln(\lambda_1/\lambda_2)$. For AERONET and the model $\lambda_1 = 0.44$, $\lambda_2 = 1.02$ μm. The Ångström exponent derived from the optical thickness measurements, α, is also shown.

5. Aerosol radiative impact at the surface

The measurements of attenuation of the solar radiation reaching the surface by aerosol were given in Fig. 5 and Table 2. Here they are used to calculate the radiative impact of aerosol at the surface. Calculations of the attenuation of the entire solar flux by the aerosol are performed assuming that the spectral dependence of the optical thickness can be described by the Ångström exponent, α: $\tau_\lambda = \tau_{0.67}(0.67/\lambda)^\alpha$. It is assumed that the exponent b_λ is proportional to the path of sunlight through the atmosphere: $1/\cos(\theta_0)$, where θ_0 is the solar zenith angle. b_λ is measured for solar zenith angle of 50°. Therefore the impact at the surface is given by the integral

$$F(\theta_0) = \int F_{0\lambda} T_\lambda(\theta_0) \exp[-b_\lambda (0.66/\lambda)^\alpha \cos(50°)/\cos(\theta_0)] d\lambda, \quad (11)$$

where T_λ is the spectral transmission through the atmosphere due to gaseous absorption. We did not detect a regular variation of b_λ as a function of the wavelength. Therefore we used the spectral average value of b_λ for each site for the entire solar spectrum.

The results are summarized in Table 3, for the spectrally averaged values of the exponent b_λ. Both the model value of b_λ and the measured values are used in the calculations. The calculations were performed for solar zenith angles every 10°. Assuming equal probability of all solar zenith angles, the table also averages the aerosol radiative impact over the 24 hours. The results are plotted in Fig. 7 as a function of the spectrally average value of b_λ. In all cases the measured flux attenuation is smaller than in the model, but the difference is striking for measurements of urban–industrial pollution in GSFC. The radiative impact by the aerosol due to the attenuation of total sun light for unit optical thickness as measured (or modeled) is -81 (-105) W m^{-2} for smoke, -80 (-90) W m^{-2} for dust, and -80 (-98) W m^{-2} for urban–industrial aerosol in France but only -48 (-98) W m^{-2} for urban–industrial aerosol in Maryland. Note the large difference from the modeled results for the Maryland site.

6. Discussion and conclusions

A new technique was demonstrated to derive the solar diffuse spectral flux reaching the surface from principal-plane radiances measured by the AERONET sun/sky radiometers. While this is not a direct measurement of the flux, the flux can be derived from the principal-plane

Unauthenticated | Downloaded 06/16/21 08:18 PM UTC

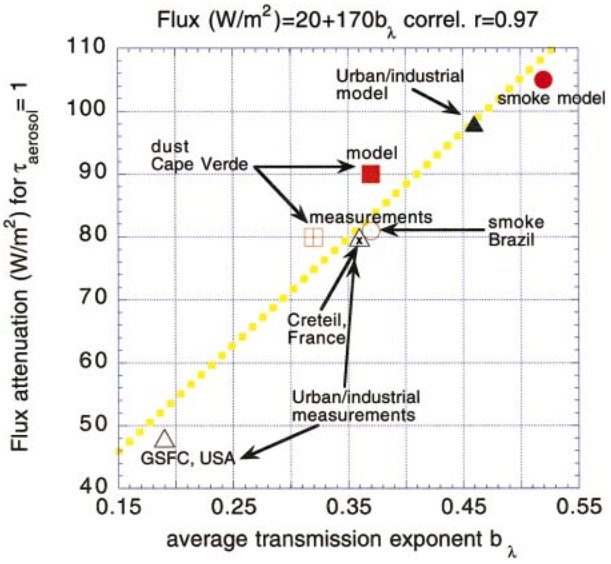

FIG. 7. Summary of the aerosol effect on flux attenuation at the surface, as function of the exponent β given in Table 2. The model results are given by full symbols and the measurements by the empty symbols. Note that the Ångström exponent, α, is different for the different models: $\alpha = 1.8$ for smoke and urban pollution and 0.5 for dust. The dashed line is the square fit to all the points. In all cases the measured flux attenuation is smaller than in the model, but the difference is striking for measurements of urban–industrial pollution in GSFC.

radiation field within 2.5%. This is in addition to the calibration error estimated to be around 5%. The advantage of the technique is the use of an existing network with 6 years of data from 50–100 instruments, better cloud screening that allows the derivation of the aerosol effect also in the presence of some cloudiness and smaller sensitivity to horizon uniformity and instrumental angular response. Application of the technique to several sites show some interesting differences from aerosol models.

While our models predict that the attenuation of total sunlight reaching the surface should be between -90 and -105 W m^{-2}, with the lowest attenuation for dust and highest for smoke, the measurements indicate -80 W m^{-2} in all the cases except for GSFC near Washington, D.C. The fact that observations of varying aerosol type give the same attenuation is surprising. Apparently the differences between these aerosol types in single scattering albedo cancel out the differences in particle effective radius. For example, smoke—due to its small particle size (effective radius of 0.14 μm; Remer et al. 1998)—does not interact effectively with solar radiation for wavelengths above 1 μm, while dust interacts with the whole solar spectrum (effective radius of 1–3 μm; Tanré et al. 2000). However, smoke single scattering albedo is 0.85 to 0.90 (Kaufman et al. 1998), while dust single scattering albedo is close to 1.0 for the solar spectrum above 0.55 μm (Tanré et al. 2001). The smaller dust absorption reduces its effect on the solar radiation near the surface. Apparently these two processes cancel each other in the present case. The value of -80 W m^{-2} is similar also to the forcing measured in the Indian Ocean Experiment (INDOEX) (Satheesh and Ramanathan 2000). The higher modeled radiative forcing at the surface (Table 3) is the result of the higher attenuation coefficients (Table 2). These theoretical attenuation coefficients are uncertain. An uncertainty in the single scattering albedo of $\Delta\omega_0 = \pm 0.05$ corresponds to an uncertainty in the attenuation coefficient $b_\lambda = \pm 0.04$ for solar zenith angle of 50° or ± 7 W m^{-2} in the daily flux at the surface (based on the equation in Fig. 7). Uncertainty in the particle size and dust nonsphericity will add to these uncertainties. In the case of smoke (see Figs. 3 and 4) the model underestimates the diffuse flux

TABLE 3. The attenuation of solar flux reaching the surface by the aerosol for optical thickness of 1.0 at 0.67 μm. The solar radiation reaching the surface was modeled using the tropical atmosphere gaseous attenuation. The attenuation of solar radiation is expressed in units of W m^{-2}. The results are give for the full solar spectrum. For each model or measurement dataset the Ångström exponent α and the attenuation coefficient b_λ are given.

	Smoke		Dust		Urban–industrial	
Parameter	Model	Measured	Model	Measured	Model	Measured, GSFC
α	1.8	1.8	0.5	0.5	1.8	1.8
b_λ	0.52	0.37	0.37	0.32	0.46	0.19
Solar zenith angle			Attenuation			
0°	259	194	216	189	233	106
10°	259	194	216	189	233	106
20°	258	194	216	189	233	108
30°	257	195	216	189	232	109
40°	253	194	214	189	289	114
50°	245	190	210	188	223	116
60°	230	183	201	181	211	114
70°	199	165	181	165	185	108
80°	134	119	130	122	128	87
90°	0	0	0	0	0	0
24-h average	105	81	90	80	98	48

Unauthenticated | Downloaded 06/16/21 08:18 PM UTC

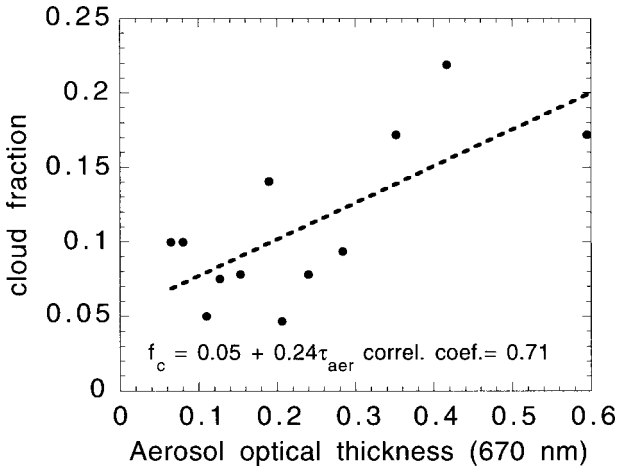

FIG. 8. Variation of the broken cloud fraction with the aerosol optical thickness in the northeast United States. Cloud data are from four locations from Virginia to New Jersey. The optical thickness measurements were located 1–60 km from the cloud observations. The data were first sorted by increasing optical thickness and then averaged in groups of 8. The cloud fraction is correlated here with the aerosol optical thickness, varying from 0.05 for no aerosol to 0.3 for aerosol optical thickness of 0.6 at 670 nm. The measurements were collected during the Sulfates, Clouds and Radiation—Atlantic (SCAR-A) experiment in 1993 (Remer et al. 1997).

to the surface for high optical thickness. This is expected due to the increase of the smoke single scattering albedo and particle size as a function of the smoke optical thickness (Kaufman et al. 1998).

In GSFC we measured much lower attenuation than expected from the model calculations and much smaller than the attenuation in Créteil near Paris. We attribute this difference to the presence of broken clouds in the GSFC and the entire northeast United States in the summer, with a cloud fraction that is correlated with the presence of the aerosol (or optical thickness). These clouds, although eliminated from the direct field of view, can illuminate the principal plane from the side, and trap sunlight between the cloud layer and the surface, thereby increasing the solar flux reaching the surface. Monte Carlo calculations for a similar cloud effect on the brightness of a cloud-free region observed from space was presented by Kobayashi et al. (2000). The cloud fraction increases from 0.05 for low optical thickness to 0.2 for aerosol optical thickness of 0.6 at 0.67 μm (Fig. 8). We simulated the scattering among the aerosol layer, the clouds and the surface in the presence of variation in the cloud fraction, using a simple back of the envelop model (see appendix) that models the effect of the change in the cloud fraction as a function of the aerosol optical thickness. Clouds scattered direct sunlight and sunlight reflected from the surface. The extra photons that are scattered from the clouds illuminated the aerosol and molecular column in the cloud-free region, and contributed the extra energy that compensated partially for the aerosol attenuation. The increase in the cloud fraction and the cloud effect, compensates partially for the reduction in the irradiance of the surface by the increase in aerosol backscattering to space and aerosol absorption. The results are demonstrated in Fig. 9 and compared with the measurements. The cloud effect reduced the aerosol attenuation coefficient on average by factor of 2. This lower value is similar to the present measurements in GSFC and represents an interesting interaction among change in haziness, correlated change in fraction of broken cloudiness

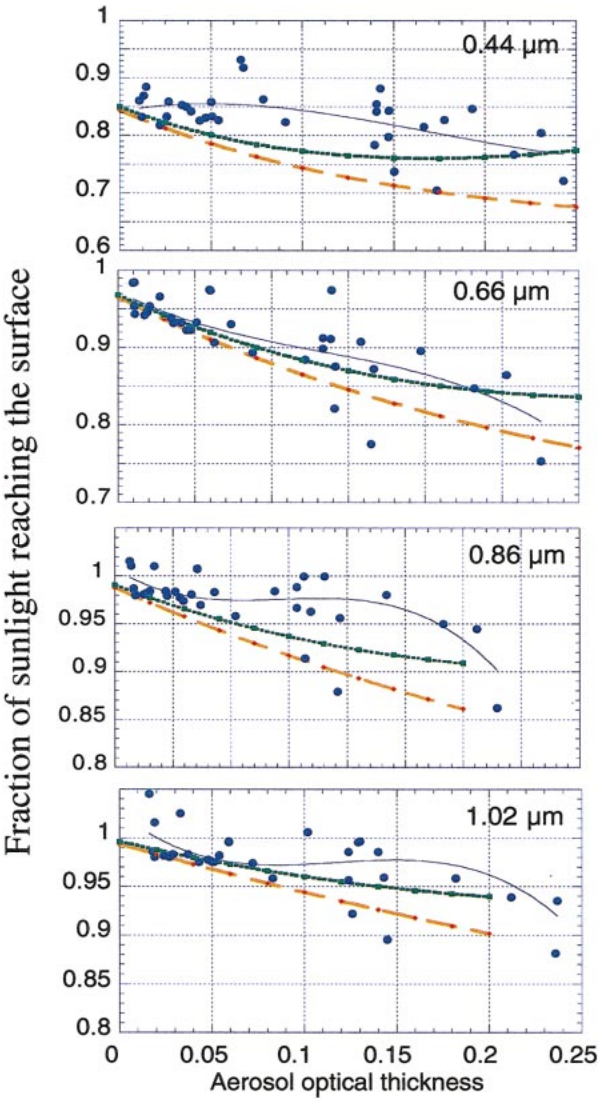

FIG. 9. Demonstration of the effect of broken cloudiness on the downward flux at the surface. Blue points are AERONET measurements of the fraction of sunlight reaching the surface as a function of the aerosol optical thickness. Red and green lines are the calculations, respectively, without and with a change in cloud fraction from 0.05 to 0.3 with the change in the optical thickness. The four panels are for wavelengths of 0.44 μm at the top to 1.02 μm at the bottom. The cloud effect—the green line explains to a large degree the lack of decrease in the fraction of photons reaching the surface with an increase in the aerosol optical thickness.

Unauthenticated | Downloaded 06/16/21 08:18 PM UTC

and the radiation field, that we did not find in other locations.

In calculating the integral on the solar spectrum, we assumed that we can use spectrally constant values of the Ångström exponent α and of the aerosol attenuation coefficient b. Spectral measurements of the sky radiance in a wider spectral range are needed to improve beyond this assumption. However, in most cases the aerosol forcing for wavelengths >1 μm is small and the assumptions are not expected to introduce a significant errors.

Acknowledgments. We would like to acknowledge the AERONET and PHOTON networks that provided the data. We also wish to express our gratitude to the director of the Servico National de Meteorologia e Geophysica (SNMG), Cape Verde for hosting and maintaining the AERONET site.

APPENDIX

Back of the Envelope Calculations of the Effect of a Broken Cloud Field on the Surface Irradiance

a. Cloud free

The fraction of sunlight reaching the surface in a cloud-free atmosphere, $F_{\text{cloud-free}}$ in a given spectral region can be approximated by

$$F_{\text{cloud-free}} = F_{\text{dirct}} + F_{\text{diffuse}} + F_{\text{multi-ref-aer}}. \quad \text{(A1)}$$

Here, F_{dirct} is the direct solar radiation reaching the surface:

$$F_{\text{dirct}} = \exp(-\tau/\mu_0),$$

where τ is the total optical thickness and μ_0 is cosine of the solar zenith angle.

For F_{diffuse} minus the diffuse radiation reaching the surface:

$$F_{\text{diffuse}} = \beta_{\text{forward-total}}(1 - F_{\text{direct}}),$$

where $\beta_{\text{forward-total}} = (\beta_{\text{forward-aerosol}}\tau_{\text{aerosol}} + 0.5\tau_{\text{Rayleigh}})/\tau$, $\beta_{\text{forward-aerosol}}$ is the fraction of photons that interact with the aerosol and are scattered forward, τ_{aerosol} is the aerosol optical thickness, 0.5 is the fraction of photons scattered forward by molecular Rayleigh scattering, and τ_{Rayleigh} is their optical thickness.

The $F_{\text{multi-ref}}$ is multiple scattering between the surface and atmosphere:

$$F_{\text{multi-ref}} = (F_{\text{dirct}} + F_{\text{diffuse}})\rho_s R_{\text{atm}},$$

where $R_{\text{atm}} = \beta_{\text{back-total}}\tau/2$.

b. Adding clouds

The fraction of sunlight reaching the surface in a cloud-free spot, in the presence of broken cloudiness with cloud fraction f_c, cloud transmission t_c, and cloud reflection R_c, is $F_{+\text{cloud}}$, approximated by

$$F_{+\text{cloud}} = F_{\text{cloud-free}} + F_{\text{cloud-trans}} + F_{\text{cloud-ref}} + \Delta F_{\text{multi-ref}}. \quad \text{(A2)}$$

Here assume that the diffuse radiation in the sunny pixel is not affected by the obscuration by clouds of part of the sky due to the strong forward structure of the diffuse radiation, and therefore the cloud effect is only in adding illumination.

The $F_{\text{cloud-trans}}$ minus diffuse light transmitted through the cloud layer and scattered in the atmosphere to the sensor is

$$F_{\text{cloud-trans}} = f_c t_c (F_{\text{direct}} + F_{\text{diffuse}})\beta_{\text{forward-total}}\tau.$$

The $F_{\text{cloud-ref}}$ minus light backscattered by the atmosphere (R_{atm}) and reflected downward by the cloud layer (R_c) is

$$F_{\text{cloud-ref}} = R_{\text{atm}} f_c (1 - f_c) R_c,$$

where $\beta_{\text{back-total}}$ is similar to $\beta_{\text{back-total}}$ replacing the aerosol forward scattering fraction with the backscattering.

The $\Delta F_{\text{multi-ref}}$ − light reflected by the surface (ρ_s) and reflected downward by the cloud layer is

$$\Delta F_{\text{multi-ref}} = (T_{\text{cloud-free}} + f_c t_c)\rho_s [R_c f_c + R_{\text{atm}}(1 - f_c)] - F_{\text{multi-ref}}.$$

REFERENCES

Ackerman, A. S., Q. B. Toon, D. E. Stevens, A. J. Heymsfield, V. Ramanathan, and E. J. Welton, 2000: Reduction of tropical cloudiness by soot. *Science,* **288,** 1042–1047.

Alpert, P., Y. J. Kaufman, Y. Shay-El, D. Tanre, A. da Silva, S. Schubert, and Y. H. Joseph, 1998: Quantification of dust-forced heating of the lower troposphere. *Nature,* **395,** 367–370.

Arking, A., 1996: Absorption of solar energy in the atmosphere: Discrepancy between model and observations. *Science,* **273,** 779–782.

Belmiloud, D., R. Schermaul, K. M. Smith, N. F. Zobov, J. W. Brault, R. C. M. Learner, D. A. Newnham, and J. Tennyson, 2000: New studies of the visible and near-infrared absorption by water vapour and some problems with the HITRAN database. *Geophys. Res. Lett.,* **27,** 3703–3706.

Bird, R. E., and C. Riordan, 1986: Simple solar spectral model for direct and diffuse irradiance on horizontal and tilted planes at the earth's surface for cloudless atmospheres. *J. Climate Appl. Meteor.,* **25,** 87–97.

Bush, B. C., and F. P. J. Valero, 1999: Comparison of ARESE clear sky surface radiation measurements. *J. Quant. Spectrosc. Radiat. Transfer,* **61,** 249–264.

Cess, R. D., and Coauthors, 1995: Absorption of solar radiation by clouds—Observations versus models. *Science,* **267,** 496–499.

Charlock, T. P., and T. L. Alberta, 1996: The CERES/ARM/GEWEX experiment (CAGEX) for the retrieval of radiative fluxes with satellite data. *Bull. Amer. Meteor. Soc.,* **77,** 2673–2683.

Charlson, R. J., S. E. Schwartz, J. M. Hales, R. D. Cess, J. A. Coakley Jr., J. E. Hansen, and D. J. Hofman, 1992: Climate forcing of anthropogenic aerosols. *Science,* **255,** 423–430.

Christopher, S. A., M. Wang, T. A. Berendes, R. M. Welch, and S. K. Yang, 1998: The 1985 biomass burning season in South America: Satellite remote sensing of fires, smoke, and regional radiative energy budgets. *J. Appl. Meteor.,* **37,** 661–678.

Dave, J. V., and J. Gazdag, 1970: A modified Fourier transform meth-

Unauthenticated | Downloaded 06/16/21 08:18 PM UTC

od for multiple scattering calculations in a plane parallel Mie atmosphere. *Appl. Opt.*, **9,** 1457–1466.

Dubovik, O., A. Smirnov, B. N. Holben, M. D. King, Y. J. Kaufman, T. F. Eck, and I. Slutsker, 2000: Accuracy assessment of aerosol optical properties retrieval from AERONET sun and sky radiance measurements. *J. Geophys. Res.*, **105,** 9791–9806.

Eck, T. F., B. N. Holben, I. Slutsker, and A. Setzer, 1998: Measurements of irradiance attenuation and estimation of aerosol single scattering albedo for biomass burning aerosols in Amazonia. *J. Geophys. Res.*, **103,** 31 865–31 878.

Hansen, J. E., and L. D. Travis, 1974: Light scattering in planetary atmospheres. *Space Sci. Rev.*, **16,** 527–610.

Harrison, L., J. Michalsky, and J. Berndt, 1994: Automatic multifilter rotating shadow-band radiometer: An instrument for optical depth and radiation measurements. *Appl. Opt.*, **33,** 5118–5125.

Hegg, D. A., J. Livingston, P. V. Hobbs, T. Novakov, and P. Russell, 1997: Chemical apportionment of aerosol column optical depth off the mid-Atlantic coast of the United States. *J. Geophys. Res.*, **102,** 25 293–25 303.

Herman, J. R., P. K. Barthia, O. Torres, C. Hsu, C. Seftor, and E. Celarier, 1997: Global distribution of UV absorbing aerosol from Nimbus 7 TOMS data. *J. Geophys. Res.*, **102,** 16 911–16 922.

Herman, M., J. L. Deuzé, C. Devaux, P. Goloub, F. M. Bréon, and D. Tanré, 1997: Remote sensing of aerosol over land surfaces including polarization measurements and application to POLDER measurements. *J. Geophys. Res.*, **102,** 17 039–17 050.

Higurashi, A., and T. Nakajima, 1999: Development of a two-channel aerosol retrieval algorithm on a global scale using NOAA AVHRR. *J. Atmos. Sci.*, **56,** 924–941.

Holben, B. N., and Coauthors, 1998: AERONET—A federated instrument network and data archive for aerosol characterization. *Remote Sens. Environ.*, **66,** 1–16.

Husar, R. B., J. Prospero, and L. L. Stowe, 1997: Characterization of tropospheric aerosols over the oceans with NOAA Advanced Very High Resolution Radiometer optical thickness operational product. *J. Geophys. Res.*, **102,** 16 889–16 909.

Kaufman, Y. J., and B. N. Holben, 1996: Hemispherical backscattering by biomass burning and sulfate particles derived from sky measurements. *J. Geophys. Res.*, **101,** 19 433–19 445.

——, and Coauthors, 1997a: Passive remote sensing of tropospheric aerosol and atmospheric correction. *J. Geophys. Res.*, **102,** 16 815–16 830.

——, D. Tanré, L. Remer, E. Vermote, A. Chu, and B. N. Holben, 1997b: Remote sensing of tropospheric aerosol from EOS-MODIS over the land using dark targets and dynamic aerosol models. *J. Geophys. Res.*, **102,** 17 051–17 067.

——, and Coauthors, 1998: The Smoke, Clouds, and Radiation—Brazil (SCAR-B) experiment. *J. Geophys. Res.*, **103,** 31 783–31 808.

King, M. D., 1979: Determination of the ground albedo and the index of absorption of atmospheric particulates by remote sensing. Part II: Application. *J. Atmos. Sci.*, **36,** 1072–1083.

Kobayashi, T., K. Masuda, M. Sasaki, and J. Mueller, 2000: Monte Carlo simulations of enhanced visible radiance in clear-air satellite fields of view near clouds. *J. Geophys. Res.*, **105,** 26 569–26 576.

Li, Z., H. W. Barker, and L. Moreau, 1995: The variable effect of clouds on atmospheric absorption of solar radiation. *Nature*, **376,** 486–490.

——, L. Moreau, and A. Arking, 1997: On solar energy disposition: A perspective from observation and modeling. *Bull. Amer. Meteor. Soc.*, **78,** 53–70.

Marshak, A., A. Davis, W. Wiscombe, and R. Cahalan, 1997: Inhomogeneity effects on cloud shortwave absorption measurements: Two-aircraft simulations. *J. Geophys. Res.*, **102,** 16 619–16 637.

Nakajima, T., and Coauthors, 1999: Early phase analysis of OCTS radiance data for aerosol remote sensing. *IEEE Trans. Geosci. Remote Sens.*, **37,** 1575–1585.

Pilewskie, P., A. F. H. Goetz, D. A. Beal, R. W. Bergstrom, and P. Mariani, 1998: Observations of the spectral distribution of solar irradiance at the ground during SUCCESS. *Geophys. Res. Lett.*, **25,** 1141–1144.

Pinker, R. T., and I. Laszlo, 1992: Modeling surface solar irradiance for satellite applications on a global scale. *J. Appl. Meteor.*, **31,** 194–211.

Ramanathan, V., B. Subasilar, G. J. Zhang, W. Conant, R. D. Cess, J. T. Kiehl, H. Grassl, and L. Shi, 1995: Warm pool heat budget and shortwave cloud forcing—A missing physics? *Science*, **267,** 499–503.

Remer, L. A., and Y. J. Kaufman, 1998: Dynamical aerosol model: Urban/industrial aerosol. *J. Geophys. Res.*, **103,** 13 859–13 871.

——, S. Gassó, D. Hegg, Y. J. Kaufman, and B. N. Holben, 1997: Urban/industrial aerosol: Ground-based sun/sky radiometer and airborne in situ measurements. *J. Geophys. Res.*, **102,** 16 849–16 859.

——, Y. J. Kaufman, B. N. Holben, A. M. Thompson, and D. McNamara, 1998: Tropical biomass burning smoke aerosol size distribution model. *J. Geophys. Res.*, **103,** 31 879–31 892.

Satheesh, S. K., and V. Ramanathan, 2000: Large differences in tropical aerosol forcing at the top of the atmosphere and Earth's surface. *Nature*, **405,** 60–63.

Shaw, G. E., 1979: Inversion of optical scattering and spectral extinction measurements to recover aerosol size spectra. *Appl. Opt.*, **18,** 988–993.

Stephens, G. L., and S.-C. Tsay, 1990: On the cloud absorption anomaly. *Quart. J. Roy. Meteor. Soc.*, **116,** 671–704.

Tanré, D., Y. J. Kaufman, M. Herman, and S. Mattoo, 1997: Remote sensing of aerosol over oceans from EOS-MODIS. *J. Geophys. Res.*, **102,** 16 971–16 988.

——, and Coauthors, 2001: Climatology of dust aerosol size distribution and optical properties derived from remotely sensed data in the solar spectrum. *J. Geophys. Res.*, **106,** 18 205–18 217.

Vogelmann, A. M., V. Ramanathan, W. C. Conant, and W. E. Hunter, 1998: Observational constraints on non-Lorentzian continuum effects in the near-infrared solar spectrum using ARM ARESE data. *J. Quant. Spectrosc. Radiat. Transfer*, **60,** 231–246.

Unauthenticated | Downloaded 06/16/21 08:18 PM UTC